Available online at www.sciencedirect.com

ScienceDirect

Physics Procedia 7 (2010) 52–62

Physics Procedia

www.elsevier.com/locate/procedia

Universality of the evaporation/condensation transition

Andreas Nußbaumer[a], Elmar Bittner[a], Thomas Neuhaus[b], and Wolfhard Janke[a]

[a]*Institut für Theoretische Physik and Centre for Theoretical Sciences (NTZ), Universität Leipzig, Postfach 100 920, D-04009 Leipzig, Germany*
[b]*John von Neumann-Institut für Computing, Forschungszentrum Jülich, D-52425 Jülich, Germany*

Abstract

By making use of the well-known lattice-gas interpretation, we investigated the evaporation/condensation transition through Monte Carlo simulations of the square lattice Ising model with nearest-neighbour couplings and periodic boundary conditions. The particle density can be varied by choosing different fixed magnetisations. In the analysis of our data we followed recent analytical work by Biskup *et al*. [*Europhys. Lett.* 60 (2002) 21], who also used the Ising model to study liquid-vapour systems at a fixed excess δN of particles above the ambient gas density in the limit of large system sizes. By identifying a dimensionless parameter $\Delta(\delta N)$, they showed that for $\Delta < \Delta_c$ all excess is absorbed in background fluctuations ("evaporated" system), while for $\Delta > \Delta_c$ a single large droplet of the dense phase occurs ("condensed" system). Besides the threshold value Δ_c also the fraction λ of excess particles forming the droplet is given explicitly.

To test the applicability of these asymptotic results to practically accessible system sizes, we measured the volume of the largest minority droplet, corresponding to a fluid drop, for various $L \times L$ lattices with $L = 40, \ldots, 640$. Using analytic values for the spontaneous magnetisation m_0, the susceptibility χ and the Wulff interfacial free-energy density τ_W for the infinite system, we were able to determine Δ_c and λ numerically in very good agreement with the theoretical prediction. We also discuss the associated free-energy barrier and its implication for multimagnetical simulations, and put these findings into context with the related droplet/strip transition respectively barrier.

Keywords: lattice gas, droplet condensation, Ising model, Monte Carlo simulations

1. Introduction

One still very challenging problem in the equilibrium statistical physics of first-order phase transitions is the "birth" of droplets containing the "wrong phase" and the reverse evaporation process. Being one of the classical problems of statistical physics, this evaporation/condensation phenomenon has been studied over the years by many authors. Early contributions are the seminal analytical work by Fisher [1] and first numerical studies by Binder, Kalos and Furukawa [2, 3]. Recently this problem has been reconsidered by Hager and one of the authors [4] with emphasis on implications of the associated nucleation barrier for the performance of computer simulation studies. This stimulated further new theoretical [5, 6, 7] and numerical [8] work. In particular the theoretical framework of Biskup *et al*. [5, 6] provides a proper equilibrium theory which does not need to explicitly involve subtle correction effects a la Gibbs-Thomson or Tolman [9], as discussed in many earlier papers [10]. Here we follow their formulation which leads to model independent scaling predictions for the evaporation/condensation transition in the infinite-volume limit.

One purpose of our study was to investigate by how much these asymptotic predictions are affected by finite-size effects. The second goal was to test the degree of universality suggested by the analytical treatment. After first describing in Sect. 2 the physical picture of the evaporation/condensation and the related droplet/strip transitions in some

1875-3892
doi:10.1016/j.phpro.2010.09.044

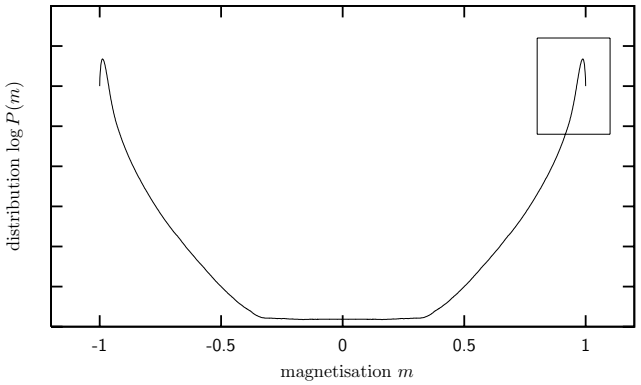

Figure 1: Probability density of the magnetisation in an Ising model below the Curie temperature T_c. The marked box indicates the region where the evaporation/condensation transition takes place. The crossover to the flat bottom at around $m_{\|} = \pm 0.35$ is often referred to as the droplet/strip transition.

detail and explaining its implications for the efficiency of numerical simulations, in particular in the multicanonical ensemble, the analytical predictions of Biskup *et al.* [5, 6] are summarized in Sect. 3. In Sect. 4 we discuss the results of our quite extensive simulations, and in Sect. 5 the paper closes with a few concluding remarks.

2. Physical picture

The paradigm for the evaporation/condensation phenomenon is the decay or growth of a fluid droplet in the gas phase, but there are also many other systems for which the basic physical mechanism is similar. Here, we will focus on the lattice-gas interpretation of the standard nearest-neighbour Ising model with Hamiltonian

$$\mathcal{H} = -J \sum_{\langle i,j \rangle} \sigma_i \sigma_j \,, \quad \sigma_i = \pm 1 \,, \quad J = 1 \,, \tag{1}$$

where the central object is a "−" Ising droplet in the bulk phase of "+" spins (or vice versa). For a large but finite system of V spins in zero magnetic field at a given temperature T below the Curie temperature T_c, the equilibrium probability distribution of the magnetisation per spin, $m = \sum_i \sigma_i / V$, exhibits the typical double-peak structure depicted in Fig. 1. The marked box highlights the region we are mainly interested in. The peak is located close to the infinite-volume equilibrium magnetisation m_0. Since $m < 1$ for any non-zero temperature, the corresponding spin configurations must contain in equilibrium on average a certain fraction n_- of overturned spins: $M = Vm = n_+ - n_- = V - 2n_-$, where $V = n_+ + n_-$, i.e., $n_-/V = (1 - m)/2$. In the lattice-gas interpretation, this determines the equilibrium particle density $\rho \equiv n_-/V$ at a given temperature T, with a small magnetisation m corresponding to a high density ρ and vice versa.

Equilibrium fluctuations in finite systems can thus drive the magnetisation away from $m \approx m_0$, respectively the particle density away from $\rho \approx \rho_0$. Note that while the magnetic Ising system is handled in the canonical formalism, this corresponds in the lattice-gas picture to a grand-canonical ensemble in which the particle number is allowed to vary. For $m < m_0$ more spins are overturned and some small bubbles of the "wrong" phase start to grow. When m decreases further, their number and size increases and, at a fixed magnetisation (or particle density in the lattice-gas interpretation), it is the balance between interaction energy and entropy which decides how a typical spin configuration looks like. A gas of many relatively small and well separated bubbles has a high entropy but costs a lot of energy since many bonds are broken. It may be thus favorable to combine several of these small bubbles to a relatively large droplet where less bonds are broken. On the other hand, configurations with such a condensed nucleus of the "wrong" phase plus only a few small bubbles have of course a smaller translational entropy since less objects can be moved around. Which of the two scenarios finally wins depends, at a given temperature, crucially on the

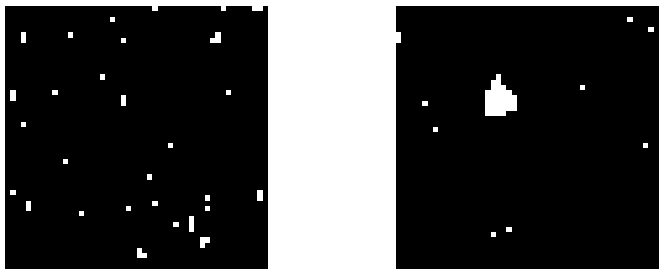

Figure 2: Two snapshots of a $L = 50$ system for $T = 1.5$ at the evaporation/condensation magnetisation m_c. *Left*: Evaporated system with a large number of very small bubbles (1 to 3 spins). *Right*: Condensed system with a single large droplet that has absorbed nearly all small bubbles.

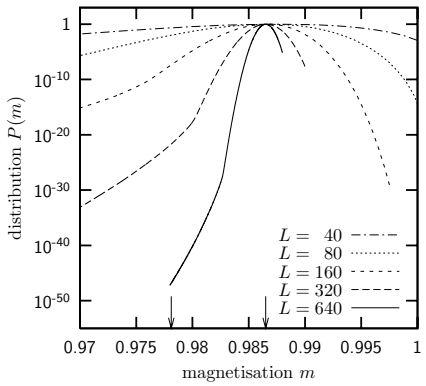

Figure 3: Probability density of the magnetisation around the right peak of Fig. 1 for different system sizes L on a linear-log scale. The cusp indicates the evaporation/condensation transition region. On the right side of the cusp (evaporated system) a Gaussian peak is clearly visible, while on the left side (condensed system) a stretched exponential behaviour can be seen. The two arrows on the x-axis indicate for $L = 640$ the range of data points used later in Fig. 11.

magnetisation (particle density). If the magnetisation m is larger than some critical value m_c (low particle density), then the evaporated phase with many small bubbles is stable, and if m is smaller than m_c (high particle density), the condensed phase consisting of one large droplet plus a few small bubbles wins. The decisive magnetisation m_c is the celebrated evaporation/condensation point. Varying m (the particle density) across m_c, the system experiences a first-order like transition with a typical double-peak structure in the droplet-size distribution right at m_c, indicating phase coexistence between the evaporated and condensed phase. This physical picture is illustrated in Fig. 2 where for a relatively small lattice two configurations found in simulations at the transition point m_c are shown. Note that even though the plots show configurations that actually occurred during the simulation, they give a slightly biased picture since for the condensed system we have picked an extreme case as far as the size of the largest droplet is concerned. In the magnetisation distribution of Fig. 1, the evaporation/condensation transition is signalised by a cusp at m_c, which is roughly located at the point where the peak around m_0 ceases to display a Gaussian shape. This can be be seen more clearly in Fig. 3, where only the marked region around the right peak of Fig. 1 is shown for various lattice sizes.

With further decreasing magnetisation (increasing particle density), the droplet grows and absorbs more and more of the small bubbles until a typical configuration consists of a single more or less spherical droplet of "wrong" magnetisation $m \approx -m_0$ in the $+m_0$ background. The dominant feature is now the interface free energy of the droplet which leads to the stretched exponential behaviour of $P(m)$ for $m < m_c$ in Figs. 1 and 3. Decreasing m further, the single large droplet of the "wrong" "$-$" phase continues growing until at another critical magnetisation $m_{\|}$ it percolates

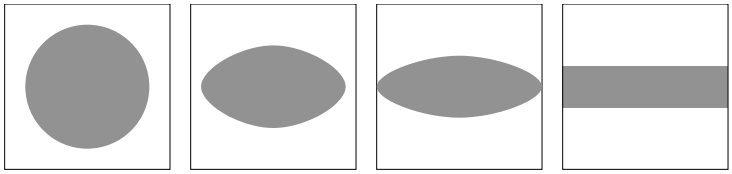

Figure 4: Optimal transition path from the spherical droplet via two circular arcs to the strip configuration at fixed magnetisation (particle density). The free-energy barrier in between scales with the lattice size L as $\Delta F \approx 0.1348 \times 2\sigma L$.

the finite system in the droplet/strip transition. The latter transition is much more pronounced and clearly indicated in Fig. 1 by the beginning of the flat region around $m = 0$.

Assuming an isotropic interface tension σ and hence an approximately spherical droplet the location of $m_\parallel$ can be easily explained as follows. For a configuration containing one large droplet of radius R (and "wrong" magnetisation density $-m_0$), the total magnetisation is $M_{\text{droplet}} = m_0(L^2 - 2\pi R^2)$ and the free energy becomes $F_{\text{droplet}} = F_0 + 2\pi R\sigma$, where we have assumed a two-dimensional system and F_0 is the bulk contribution to the free energy. For a percolating strip of magnetisation $-m_0$ of width w one finds similarly $M_{\text{strip}} = m_0(L^2 - 2wL)$ and $F_{\text{strip}} = F_0 + 2L\sigma$, where we have ignored interactions between the two (on average) straight interfaces. Notice that in this approximation F_{strip} does not depend on the width w and hence the magnetisation M_{strip}, which explains the flat region in the magnetisation distribution of Fig. 1. As usual the stable configuration is the one with the smaller free energy. By equating $F_{\text{droplet}} = F_{\text{strip}}$, one easily finds the critical droplet radius $R_c = L/\pi$. Inserting this into the expression for M_{droplet}, we finally arrive at the critical magnetisation $M_\parallel \equiv M_{\text{droplet}} = (L^2 - 2L^2/\pi)\, m_0$ or

$$m_\parallel = (1 - 2/\pi)\, m_0 \approx 0.3634\, m_0\,. \tag{2}$$

For magnetisations smaller than $m_\parallel$, it is for the system hence statistically preferable to be in the strip configuration. Note, however, that the critical droplet radius at $m_\parallel$ is $R_c = L/\pi$ and hence its diameter $2R_c = 2L/\pi \approx 0.6366L < L$ is much too small to percolate the lattice. At fixed magnetisation $m_\parallel$, the droplet must hence somehow deform its shape to reach the preferable strip configuration. Such a deformation, however, can only proceed by climbing some free-energy barrier. The optimal "transition path" across this free-energy barrier was found already a while ago by Leung and Zia [11] who showed that the minimal-cost deformation of a droplet of fixed size (i.e., fixed magnetisation) consists of two circular arcs, cf. Fig. 4. At the point where the long axis of this deformed droplet approaches the lattice size L, the angle θ with the straight interface is given by the transcendental equation $\theta = ((2/\pi)\sin\theta + \cos\theta)\sin\theta \approx 0.8601$, and the maximal free-energy barrier reads

$$\Delta F = (\theta/\sin\theta - 1)2\sigma L \approx 0.1348 \times 2\sigma L\,. \tag{3}$$

This barrier plays an important role for the understanding of the dynamics of simulations in the multicanonical ensemble or, in this context, more precisely multimagnetical simulations [12]. The main ingredient of this method are iteratively determined auxiliary weight factors $W(m)$ which, when multiplied with the usual canonical Boltzmann factor, produce a flat distribution of the magnetisation between the two peaks of the canonical distribution. While canonically the probability in the region around $m = 0$ is suppressed by a factor $\exp(-2\beta\sigma L^{D-1})$ relative to the two peaks, in the multimagnetical ensemble all states are equally probable. For the canonical ensemble this implies a dramatic slowing down with an exponentially growing autocorrelation time $\tau \propto \exp(2\beta\sigma L^{D-1})$. In the multimagnetical simulations, on the other hand, one would naively expect a random walk behaviour of the Monte Carlo dynamics and hence only a power-law scaling of τ with the lattice size L [13]. Equation (3) teaches us, however, that this cannot be true at all since the system cannot easily pass through the point $m \approx m_\parallel$. Rather, it first has to overcome the free-energy barrier (3) in a direction "orthogonal" to the magnetisation which leads in two dimensions to a slowing down of the form $\tau \propto \exp(0.1348 \times 2\beta\sigma L)$. This is much weaker than the canonical slowing down $\propto \exp(2\beta\sigma L)$, but still exponentially bad. As Fig. 5 clearly demonstrates, such a slowing down due to a "hidden" free-energy barrier is indeed observed in multimagnetical simulations.

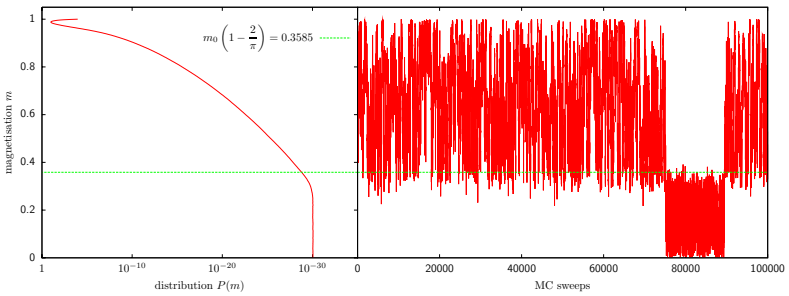

Figure 5: Time evolution of a multimagnetical Ising model simulation on a 40×40 square lattice at $T = 1.5$ and close to the droplet/strip transition point $m_{\parallel}$. One sees clearly that the system's path through the state space is usually reflected at $m \approx m_{\parallel}$ and only rarely the droplet/strip barrier (3) is overcome.

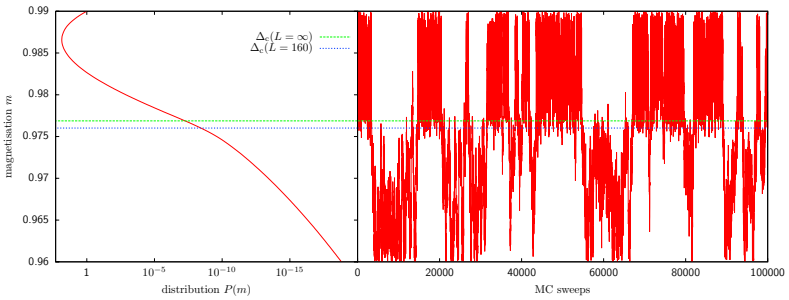

Figure 6: Similar plot to Fig. 5, again at $T = 1.5$, but here for a much bigger 160×160 square lattice close to the evaporation/condensation point m_c.

Having understood this, in the following we will concentrate on the evaporation/condensation transition, which also exhibits first-order like signatures with an associated free-energy barrier. The time series of a multimagnetical simulation around m_c in Fig. 6 shows that also this barrier has a significant impact, albeit with a much less pronounced slowing-down effect. Despite this barrier the resulting multimagnetical histogram is perfectly flat. This is demonstrated in Fig. 7, where it is also shown how the contributions from the condensed and evaporated phase add up to produce the total histogram.

3. Theory

In the following we consider the square lattice Ising model (1) in the low-temperature phase at an inverse temperature $\beta \equiv 1/T > \beta_c = \ln\left(1+\sqrt{2}\right)/2$ and assume that it is initially in the phase with positive magnetisation. The infinite-volume equilibrium magnetisation per site is denoted by $m_0 = M_0/V = m_0(\beta) > 0$. For a finite system of volume $V = L\times L$, due to fluctuations, some (possibly disconnected) volume v_L may be in the "wrong" phase with inverted spins. The magnetisation can then be decomposed as $M = m_0\,(V - v_L) - m_0 v_L$, implying

$$\delta M \equiv M - Vm_0 = -2v_L m_0\,. \tag{4}$$

As already discussed in Sect. 2, in extreme cases, this excess in magnetisation may be distributed in many small bubbles (background fluctuations) or in one large droplet. By isoperimetric reasoning, it can be shown that no droplets

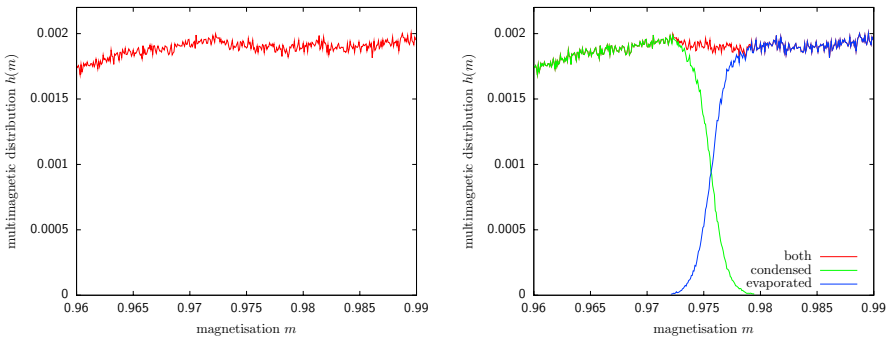

Figure 7: *Left*: Flat microcanonical histogram resulting from the time evolution shown in Fig. 5. *Right*: Decomposition of the histogram into the contributions from the condensed and evaporated phase.

of intermediate size can exist [6]. In the former case, large-deviation theory predicts a Gaussian distribution [14],

$$\exp\left[-\beta\frac{(\delta M)^2}{2\chi V}\right] = \exp\left[-\beta\frac{2m_0^2 v_L^2}{\chi V}\right], \tag{5}$$

where $\chi = \chi(\beta) = \beta V\left[\langle m^2\rangle - \langle m\rangle^2\right]$ is the susceptibility in the thermodynamic limit, while in the second case, the probability depends on the interface free energy $\tau_{\rm W}(\beta)$ per unit volume of an optimally shaped large Wulff droplet [15, 16, 17],

$$\exp\left[-\beta\tau_{\rm W}\sqrt{v_L}\right]. \tag{6}$$

In the general case, only a fraction $v_{\rm d} = \lambda v_L$ will condense forming the large droplet and the rest $v_{\rm f} = v_L - v_{\rm d} = (1-\lambda)v_L$ will contribute to the small bubble fluctuations. The probability distribution is hence in general given by an interpolation between eqs. (5) ($\lambda = 0$) and (6) ($\lambda = 1$),

$$\exp\left[-\beta\frac{2m_0^2(1-\lambda)^2 v_L^2}{\chi V} - \beta\tau_{\rm W}\sqrt{\lambda v_L}\right] = \exp\left[-\beta\tau_{\rm W}\sqrt{v_L}\Phi_\Delta(\lambda)\right], \tag{7}$$

where

$$\Phi_\Delta(\lambda) = \sqrt{\lambda} + \Delta(1-\lambda)^2, \tag{8}$$

with

$$\Delta = \frac{2m_0^2 v_L^2}{\chi V\tau_{\rm W}\sqrt{v_L}} = \frac{2m_0^2}{\chi\tau_{\rm W}}\frac{v_L^{3/2}}{V} \tag{9}$$

being a scaling parameter which depends on the model specific parameters m_0, χ, and $\tau_{\rm W}$, the volume $V = L^2$ and via eq. (4) on the magnetisation m,

$$1 - m/m_0 = 2\left(\chi\tau_{\rm W}/2m_0^2\right)^{2/3}(\Delta/L)^{2/3}. \tag{10}$$

The most probable situation at fixed Δ, i.e, constant magnetisation respectively particle density, is obtained by minimising $\Phi_\Delta(\lambda)$ as a function of the fraction $\lambda = v_{\rm d}/v_L$. Depending on the parameter Δ, the solution behaves like at a first-order phase transition: for $\Delta < \Delta_{\rm c} = (1/2)(3/2)^{3/2} \approx 0.9186$, the global minimum is reached for $\lambda = 0$, while for $\Delta > \Delta_{\rm c}$ a nontrivial solution $\lambda = \lambda(\Delta) > 0$ is found. At $\Delta = \Delta_{\rm c}$, the solution jumps to a value $\lambda_{\rm c} = 2/3$, cf. Figs. 8 and 9. At $\Delta_{\rm c}$, the large droplet thus starts to form in an abrupt, first-order transition like nucleation process. In a sense, this is a model-independent, universal result (model-dependent parameters are, however, collected in the definition (9) of the scaling parameter Δ).

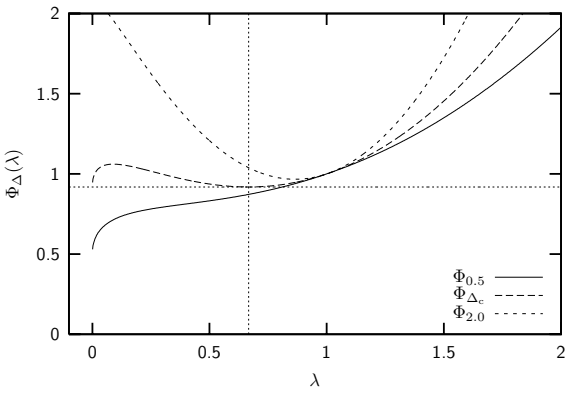

Figure 8: The function $\Phi_\Delta(\lambda)$ for three characteristic values of the parameter Δ defined in eq. (9). At $\Delta_c = (1/2)(3/2)^{3/2} \approx 0.9186$ the absolute minimum at $\lambda = 0$ for $\Delta < \Delta_c$ jumps to a non-trivial value $\lambda \geq 2/3$ (dashed vertical line) for $\Delta > \Delta_c$.

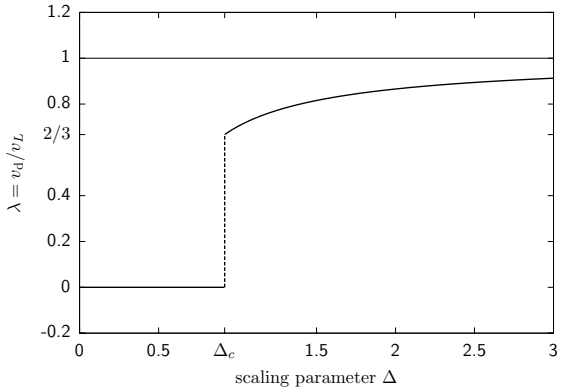

Figure 9: Analytic solution $\lambda = \lambda(\Delta)$ obtained by minimization of eq. (8).

In Fig. 8 we observe for $\Delta = \Delta_c$ a free-energy barrier which takes its maximum at $\lambda_{\max} = (2 - \sqrt{3})/3$ where $\Delta F = F_{\max} - F_{\min} = \tau_W v_L^{1/2} 3(2 - \sqrt{3})/4\sqrt{2}$. Using eq. (9) to express v_L in terms of Δ_c, we arrive at

$$\Delta F = \left(\frac{81(26\sqrt{3} - 45)}{1024} \frac{\chi \tau_W^4 V}{2m_0^2} \right)^{1/3} \approx 0.1381 \tau_W \left(\frac{\chi \tau_W}{2m_0^2} \right)^{1/3} L^{2/3} . \tag{11}$$

Inserting the parameters for the square lattice Ising model at $T = 1.5$ (see Table 1 below), one obtains the explicit result $\Delta F \approx 0.2283\, L^{2/3}$. Due to the smaller power of the lattice size L, this barrier is less severe than the droplet/strip barrier (3), but it is still clearly detectable, as is demonstrated in Fig. 6.

4. Numerical results

One aim of our Monte Carlo study [18, 19] was to investigate how fast the numerical results for finite systems approach the asymptotic theoretical predictions in the thermodynamic limit. All results reported below are from simulations at $T = 1.5 \approx 0.66\, T_c$ on square lattices of linear size $L = 40, 80, \ldots, 640$. The simulation temperature was

Table 1: Numerical values for the infinite-volume equilibrium magnetisation m_0, susceptibility χ and Wulff interface free energy per unit volume τ_W of the square lattice Ising model at the simulation temperature $T = 1.5$, entering the parameter $\Delta = \Delta(v_L, m_0, \chi, \tau_W)$ defined in eq. (9).

T	T_c	m_0	χ	τ_W	$2m_0^2/\chi\tau_W$
1.500	2.269	0.9865	0.02708	4.245	16.93

chosen as a good compromise between simulation speed (freezing of the spin-flip dynamics at too low temperatures) and compactness of the droplet (see the r.h.s. of Fig. 2 for a typical configuration).

The main observable is the fraction of excess magnetisation in the largest droplet, $\lambda = v_d/v_L$, as a function of the total volume v_L of the "wrong" phase. The total volume v_L can be tuned, via eq. (4), by the magnetisation and determines the scaling variable $\Delta = \Delta(v_L, m_0, \chi, \tau_W)$ defined in eq. (9). For the square lattice Ising model (1), two of the parameters entering here (m_0, τ_W) are known exactly and the third one (χ) can be computed with extremely high precision. The spontaneous magnetisation m_0 is given by the famous Onsager-Yang solution [20, 21]

$$m_0(\beta) = \left(1 - \sinh^{-4}(2\beta)\right)^{1/8}, \tag{12}$$

which evaluates at $T = 1.5$ to $m_0 = 0.9865\ldots$. The susceptibility is still not known exactly, but an extremely long series expansion [22],

$$\chi(\beta) = \beta \sum_{i=0}^{323} c_i u^{2i} \quad \text{with} \quad u = \frac{1}{2\sinh(2\beta)} \tag{13}$$

and $c = \{0, 0, 4, 16, 104, 416, 2224, 8896, 43840, 175296, 825648, 3300480, 15101920, ...\}$ gives the basically exact result of $\chi = 0.02708$ (the last term in eq. (13) contributes at $T = 1.5$ only $\approx 0.28 \times 10^{-158}$). Finally, for the free energy Σ_W of the Wulff droplet, Leung and Zia [11] were able to derive the analytic expression $\Sigma_W = 2\sqrt{W\Sigma}$. Here, Σ is the volume of the droplet and

$$W = \frac{4}{\beta^2} \int_0^{\beta\sigma_0} \mathrm{d}x \cosh^{-1}\left[\frac{\cosh^2(2\beta)}{\sinh(2\beta)} - \cosh(x)\right] \tag{14}$$

is the volume bounded by the Wulff plot, with $\sigma_0 = 2 + \ln[\tanh(\beta)]/\beta$ being the interface tension of an (1,0) surface (i.e., in direction of the lattice axis) [23, 24, 25]. Putting $\Sigma = 1$ gives the interfacial free energy per unit volume,

$$\tau_W(\beta) = 2\sqrt{W}, \tag{15}$$

and from a numerical integration of (14) we obtain $\tau_W = 4.245\,413\ldots$ at $T = 1.5$. Note that by assuming an isotropic interface tension σ_0 and hence a circular Wulff shape, one finds $\tau_W \approx 2\sqrt{\pi}\sigma_0 = 4.219$, which deviates from the exact result by only 0.6%. Using heuristically an average between σ_0 and the also exactly known interface tension along the diagonals, $\sigma_{\mathrm{diag}} = \sqrt{2}\ln\sinh(2\beta)/\beta$ [25], this even improves to 4.245 667 (0.006% deviation). All relevant parameters are collected in Table 1.

In a first step we determined the relevant region of the magnetisation. This was done by performing multimagnetic simulations and inspecting the distribution of the magnetisation as shown above in Fig. 3 visually. The distribution exhibits for larger lattice sizes a clear cusp around m_c which divides the evaporated and condensed region. Within the evaporated region it has a Gaussian form according to eq. (5), while in the condensed region the stretched exponential behaviour is visible, cf. eq. (6).

Next, we performed for each lattice size 38 simulations at fixed values of $\Delta_i = \{0.00, 0.10, ...\}$, i.e., at constant magnetisation, with an emphasis on the vicinity of Δ_c. The corresponding values of the total magnetisation M (cf. eq. (10)) must be rounded to the next allowed integer value and then the true Δ_i are calculated backwards. The constraint of a constant magnetisation ("micromagnetic ensemble") was enforced by utilising a Metropolis update with Kawasaki dynamics exchanging pairs of unaligned spins. Every simulation ran 20 000 sweeps for the thermalisation and 200 000 sweeps for measurements. To obtain the statistical error bars reliably, 10 independent simulations were run for each data point. After every sweep a cluster decomposition was performed using the Hoshen-Kopelman

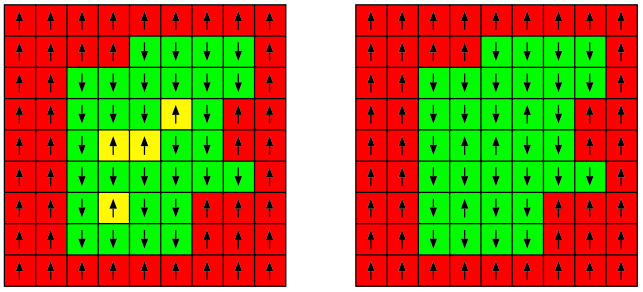

Figure 10: Sketch of a large droplet containing overturned spins in its interior (left), which must be counted when measuring its volume v_d. This is achieved by a so-called "flood-fill" algorithm (right).

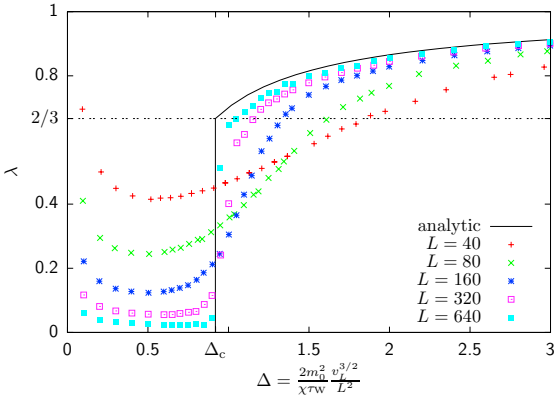

Figure 11: Fraction of excess magnetisation $\lambda = v_\mathrm{d}/v_L$ in the largest droplet of the square lattice Ising model with nearest-neighbour interactions and periodic boundary conditions for lattice sizes $L = 40, 80, \ldots, 640$ at the temperature $T = 1.5 \approx 0.66\,T_\mathrm{c}$. The error bars are not plotted since their size is much smaller than that of the data symbols. The solid line shows the analytic solution in the limit $L \to \infty$.

[26] algorithm and the volume v_d of the largest droplet was measured yielding the desired fraction λ. It should be noted that the range of magnetisations was chosen to guarantee that the droplet was always the second largest cluster (the background is the largest cluster). Also note that, in the present context, the volume or size of the cluster does include overturned spins within the cluster (in contrast to percolation studies or improved estimators in cluster-update simulations [27]), cf. Fig. 10. Our simulations are so sensitive that the proper counting of the cluster size turned out to be indeed crucial. Technically, this was handled by a so-called "flood-fill" routine [28] that ran after the Hoshen-Kopelman algorithm. In essence, it starts from an inside spin and stops when a spin that belongs to the background is reached. Very rarely ambiguous cases can occur which can be detected automatically and were taken care of by inspection.

Our main result, the fraction $\lambda = \lambda(\Delta)$ for various lattice sizes, is shown in Fig. 11. The solid line represents the analytical curve obtained by the minimization of $\phi_\Delta(\lambda)$ in eq. (8). We observe rather strong finite-size effects but for the larger lattice sizes the results of the simulations clearly approach the theoretical curve. The jump from $\lambda \approx 0$ to $\lambda \approx 2/3$ at $\Delta_\mathrm{c} \approx 0.9186$ confirms the theoretical prediction that at the evaporation/condensation transition $2/3$ of the excess of the magnetisation goes into the large droplet while the rest remains in the background fluctuations. The apparent increase of λ for $\Delta \to 0$ can be explained by the fact that the minimal cluster size is 1 and not an arbitrarily small fraction. In contrast, the excess that can be fixed analytically using eq. (9) can be much smaller than 1.

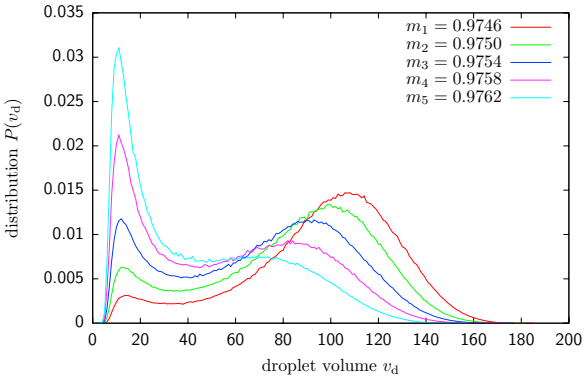

Figure 12: Size distribution of the largest droplet close to the evaporation/condensation transition on a 160×160 square lattice at $T = 1.5$, exhibiting a clear two-phase signal.

The size distribution of the largest droplet close to Δ_c respectively m_c is shown in Fig. 12 for a 160×160 lattice. One observes a clear two-phase signal: the system is either in the evaporated bubble phase with $v_d \approx 10$ or in the condensed phase consisting of one large droplet of size $v_d \approx 90$ taking up about 2/3 of the excess magnetisation. The remaining 1/3 of the excess goes into additional small bubbles not directly visible in this figure.

5. Concluding remarks

Our Monte Carlo results for the two-dimensional square lattice Ising model clearly confirm the theoretical considerations of Biskup *et al.* [5, 6] and extend their exact analysis for asymptotically large systems to practically accessible system sizes. The observed finite-size scaling behaviour matches perfectly with the predictions in the infinite-volume limit. All simulations were performed in thermal equilibrium and the suppression of droplets of intermediate size could be unambiguously confirmed. The double-peak structure of the size distribution of the largest droplet at the evaporation/condensation transition reveals a "hidden" free-energy barrier, which is shown to be also reflected by a slowing down of the performance of multimagnetical simulations.

We have also performed similar simulation studies for the standard two-dimensional Ising model on triangular lattices and with additional next-nearest neighbour interactions on square lattices [29]. While on physical grounds the results of Biskup *et al.* are of course expected to carry over to these cases as well, strictly speaking their analytical treatment in Refs. [5, 6] is confined to square lattices with nearest-neighbour couplings. Our results for these further models confirm this expectation and thus in particular provide evidence for the implied universal aspects of the theory.

Acknowledgments

We thank Kurt Binder and Roman Kotecký for useful discussions. This work was partially supported by the Deutsche Forschungsgemeinschaft (DFG) under grant Nos. JA483/22-1 & 23-1 and the EC RTN-Network "ENRAGE": *Random Geometry and Random Matrices: From Quantum Gravity to Econophysics* under grant No. MRTN-CT-2004-005616.

[1] M.E. Fisher, Rep. Prog. Phys. 30 (1967) 615.
[2] K. Binder and M.H. Kalos, J. Stat. Phys. 22 (1980) 363.
[3] H. Furukawa and K. Binder, Phys. Rev. A 26 (1982) 556.
[4] T. Neuhaus and J.S. Hager, J. Stat. Phys. 113 (2003) 47.
[5] M. Biskup, L. Chayes, and R. Kotecký, Europhys. Lett. 60 (2002) 21.
[6] M. Biskup, L. Chayes, and R. Kotecký, Comm. Math. Phys. 242 (2003) 137.
[7] K. Binder, Physica A 319 (2003) 99.

[8] P. Virnau, L.G. MacDowell, M. Müller, and K. Binder, in *Computer Simulation Studies in Condensed Matter Physics XVI*, Springer Proceedings in Physics, Vol. 95, edited by D.P. Landau, S.P. Lewis, and H.-B. Schüttler, Springer, Berlin, 2004, p. 129; L.G. MacDowell, P. Virnau, M. Müller, and K. Binder, J. Chem. Phys. 120 (2004) 5293; K. Binder, M. Müller, P. Virnau, and L.G. MacDowell, Adv. Polymer Science 173 (2005) 1.
[9] M. Biskup, L. Chayes, and R. Kotecký, J. Stat. Phys. 116 (2003) 175.
[10] J. Lee, M.A. Novotny, and P.A. Rikvold, Phys. Rev. E 52 (1995) 356; M. Pleimling and W. Selke, J. Phys. A: Math. Gen. 33 (2000) L199; M. Pleimling and A. Hüller, J. Stat. Phys. 104 (2001) 971.
[11] K. Leung and R.K.P. Zia, J. Phys. A: Math. Gen. 23 (1990) 4593.
[12] B.A. Berg and T. Neuhaus, Phys. Rev. Lett. 68 (1992) 9; B.A. Berg, U. Hansmann, and T. Neuhaus, Phys. Rev. B 47 (1993) 497; Z. Phys. B: Condens. Matter 90 (1993) 229.
[13] W. Janke, in *Computer Simulations of Surfaces and Interfaces*, NATO Science Series, II. Mathematics, Physics and Chemistry – Vol. 114, edited by B. Dünweg, D.P. Landau, and A.I. Milchev, Kluwer, Dordrecht, 2003, p. 137.
[14] Note that the β-factor in eqs. (5)–(7) was inadvertently omitted in Ref. [19].
[15] G. Wulff, Z. Kristallogr. Mineral. 34 (1901) 449.
[16] S.B. Shlosman, Comm. Math. Phys. 125 (1989) 81.
[17] R.L. Dobrushin, R. Kotecký, and S.B. Shlosman, *Wulff Construction. A Global Shape from Local Interaction*, Amer. Math. Soc., Providence, RI, 1992; J. Stat. Phys. 72 (1993) 1.
[18] A. Nußbaumer, E. Bittner, and W. Janke, PoS (LAT2005) 252.
[19] A. Nußbaumer, E. Bittner, T. Neuhaus, and W. Janke, Europhys. Lett. 75 (2006) 716.
[20] L. Onsager, Nuovo Cim. (Suppl.) 6 (1949) 261.
[21] C.N. Yang, Phys. Rev. 85 (1952) 808.
[22] W.P. Orrick, B.G. Nickel, A.J. Guttmann, and J.H.H. Perk, Phys. Rev. Lett. 86 (2001) 4120; J. Stat. Phys. 102 (2001) 795.
[23] L. Onsager, Phys. Rev. 65 (1944) 117.
[24] B.M. McCoy and T.T. Wu, *The Two-Dimensional Ising Model*, Harvard University Press, Cambridge, 1973.
[25] R.J. Baxter, *Exactly Solved Models in Statistical Mechanics*, Academic Press, New York, 1982.
[26] J. Hoshen and R. Kopelman, Phys. Rev. B 14 (1976) 3438.
[27] W. Janke, in *Ageing and the Glass Transition*, edited by M. Henkel, M. Pleimling, and R. Sanctuary, Lect. Notes Phys. 716, Springer, Berlin, 2007, p. 207.
[28] M.K. Agoston, *Computer Graphics and Geometric Modelling*, Springer, London, 2004.
[29] A. Nußbaumer, E. Bittner, and W. Janke, Phys. Rev. E 77 (2008) 041109.